

# NEW APPROACHES TO DESIGNING OF ALLOYS BASED ON $\gamma$ -TiAl+ $\alpha_2$ -Ti<sub>3</sub>Al

R.M. Imayev<sup>1</sup>, V.M. Imayev<sup>1</sup>, T.G. Khismatullin<sup>1</sup>, M. Oehring<sup>2</sup> and F. Appel<sup>1</sup>

<sup>1</sup>Institute for Metals Superplasticity Problems Russian Academy of Sciences, ul. Khalturina, 39, Ufa, 450001, Russia

<sup>2</sup>GKSS Research Center, Institute for Materials Research, Max-Planck-Str.1, D-21502 Geesthacht, Germany

Received: July 20, 2005

**Abstract.** Microstructural examination of castings of the  $\gamma$ -TiAl+ $\alpha_2$ -Ti<sub>3</sub>Al alloys depending on aluminum content, alloying additions, and cooling rate has been carried out. Experimental findings allowed a novel concept of designing of  $\gamma$ -TiAl+ $\alpha_2$ -Ti<sub>3</sub>Al alloys to be proposed. The concept is addressed on the production of cast alloys with a chemically homogeneous fine-grained microstructure and improved workability.

## 1. INTRODUCTION

Light alloys based on  $\gamma$ -TiAl+ $\alpha_2$ -Ti<sub>3</sub>Al intermetallic phases (hereafter called  $\gamma$ + $\alpha_2$  alloys) represent a unique class of materials. Owing to low density and attractive high temperature properties, they have a significant potential for innovative applications in advanced energy conversion systems, in which these materials may replace the heavier nickel-base superalloys at intended service temperatures of 600-900 °C. However, cast  $\gamma$ + $\alpha_2$  alloys have generally low ductility and damage tolerance at room temperature and low workability at elevated temperatures that restricts their application. These deficiencies are associated not only with intrinsic brittleness of the  $\gamma$  and  $\alpha_2$  phases, but also with the microstructure which evolves in castings during freezing. A coarse-grained microstructure, sharp casting texture and significant chemical inhomogeneity are typically characteristic of ingots of  $\gamma$ + $\alpha_2$  alloys [1-7]. The production of sound castings with a homogeneous fine-grained microstructure and random

texture is, therefore, of great importance for application of  $\gamma$ + $\alpha_2$  alloys. First, a widespread range of sound cast products with reproducible mechanical properties guaranteeing minimum values might be manufactured. Second, owing to increased workability of such cast materials, the fabrication of components using different hot working procedures might be significantly facilitated. However, up to now, there is no plain concept of designing of  $\gamma$ + $\alpha_2$  alloys in order to produce sound cast materials. There is still no entire understanding of microstructural evolution under freezing and cooling of  $\gamma$ + $\alpha_2$  castings depending on aluminum content, alloying additions, and cooling rate. Therefore, alloy developments have mostly been conducted by 'trial and error' basing only on general ideas of an influence of alloying additions on phase transformations and mechanical properties of  $\gamma$ + $\alpha_2$  alloys [4,6,7].

The present work is devoted to a study of the microstructure of cast  $\gamma$ + $\alpha_2$  alloys depending on the aluminum content, alloying additions and cooling

---

Corresponding author: R.M. Imayev, e-mail: renat\_imayev@mail.ru

**Table 1.** Alloy compositions and results of DSC analysis ( $T_e$ : eutectoid temperature,  $T_\alpha$ :  $\alpha$ -transus temperature).

No.	Alloy composition, at.%	$T_e$ , °C	$T_\alpha$ , °C	$T_{\alpha \rightarrow \alpha+\beta}$ , °C
1	Ti-44Al	1138	1278	1443
2	Ti-44Al-0.2B	1151	1287	1429
3	Ti-44Al-5Nb-0.2B	1161	1296	1393
4	Ti-44Al-5Nb-1Mo-0.2B-0.3C	1169	1290	1393
5	Ti-46Al-5Nb-0.2B	1168	1341	>1450

rate. Experimental findings were used to develop new  $\gamma+\alpha_2$  alloy compositions, in that good chemical homogeneity and a fine-grained microstructure were attained in as-cast condition.

## 2. EXPERIMENTAL

Buttons of about 30 g weight were melted in a laboratory arc-melting furnace on a water-cooled copper plate under argon atmosphere. The investigated materials included the alloys with varying niobium content (0, 5, 10, and 15 at.%), boron additions (0 and 0.2 at.%) and other doping elements (molybdenum, tungsten, carbon). The buttons were melted at least 7 times to ensure good homogeneity. As starting materials, high-purity metals and a Ti-49.1Al-0.37C (hereafter in at.%) master alloy were used. In the present work, 14 alloy compositions were melted and investigated. For the sake of simplicity, 5 alloys only are considered in the paper. They are listed in Table 1. Binary alloys mentioned in the paper were produced and investigated earlier [8].

Microstructural investigations were performed for as-cast conditions. Besides, some alloys were annealed at  $T=1450$  °C (5 min.), followed by furnace cooling. For microstructural and analytical investigations, the cross sections of the buttons were used. For that, the buttons were cut along their diameter. Scanning electron microscopy was performed in the back-scattering electron (BSE) mode using a Zeiss DSM962 microscope. The microscope was equipped with an energy-dispersive X-ray (EDX) analysis system (Link Oxford), which was calibrated using binary and ternary alloy standards. Experimental details on the analytical investigation can be found elsewhere [5]. Standard optical microscopy was also used for microstructural examination. Differential scanning calorimetric (DSC) analysis was carried out upon heating with a rate of 20 °C/min up to temperature of 1450 °C.

## 3. RESULTS AND DISCUSSION

### 3.1. Features of the ingot microstructure formation in binary $\gamma+\alpha_2$ alloys depending on the aluminum content

As consistent with the binary phase diagram (Fig. 1 [9]), depending on the aluminum content  $\gamma+\alpha_2$  alloys can solidify through either the peritectic reaction(s) or the solid-state  $L \Rightarrow b$  transformation. At present, alloys solidifying through the peritectic reactions are the most studied. In as-cast condition, they are characterized by a coarse colony size ( $d \gg 100$   $\mu$ m) and sharp casting texture. Such microstructure results from the  $L+\beta \Rightarrow \alpha$  peritectic reaction [4,10]. The peritectic  $\alpha$  phase is related to the  $\beta$  phase by the Burgers orientation relationship  $\{110\}_\beta // \{0001\}_\alpha$  and  $\langle 111 \rangle_\beta // \langle 11\bar{2}0 \rangle_\alpha$  that assumes the possibility of formation of 12 orientation variants of  $\alpha$ . However, under real solidification conditions, when a strong temperature gradient takes place, which gives rise to the formation of  $\beta$ -dendrites with the axis parallel to the heat-flow direction, only a single variant of the 12 is usually realized to envelop a given  $\beta$  dendrite. Further, the  $\alpha$  phase grows through  $\beta$  dendrites in such a way that coarse columnar grains with the axis  $c$  having a tendency to align parallel to the heat-flow direction finally arise. It appears to be a consequence of the low nucleation and very rapid growth rates that must accompany the high temperature solidification reaction. Upon following cooling, the solid-state  $\alpha \Rightarrow \alpha+\gamma \Rightarrow \alpha_2+\gamma$  transformations occur and all the  $\gamma$  lamellae precipitating in each columnar a grain to form the well-known  $\gamma+\alpha_2$  lamellar structure are preferably oriented perpendicularly to the hexagonal  $c$  axis because of the orientation relationship  $(0001)_\alpha // \{111\}_\gamma$  and  $\langle 11\bar{2}0 \rangle_\alpha // \langle 1\bar{1}0 \rangle_\gamma$  inherent in the transformation

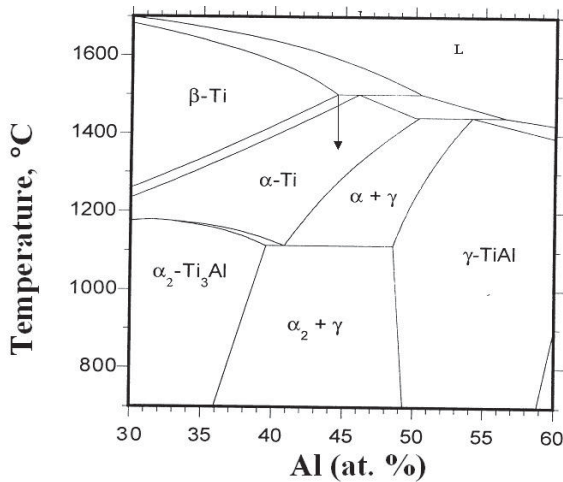


**Fig. 1.** Central portion of the binary titanium - aluminum phase diagram according to Ref. [1]. At the left side of the arrow solidification occurs completely through the  $\beta$  phase, at the right side solidification occurs through the peritectic reaction.

mechanism involved. In addition to sharp texture, solidification through the peritectic reactions is at the bottom of significant chemical inhomogeneity of  $\gamma + \alpha_2$  alloys which, as was indicated in a number of investigations, is virtually unremovable defect [1-3,5]. By way of illustration, Fig. 2a shows quantitative concentration line profile as obtained by EDX analysis demonstrating rather inhomogeneous distribution of aluminum in the upper part of the button of the Ti-48Al alloy caused by significant dendritic segregation.

In contrast to alloys solidifying through the peritectic reactions, the  $\beta$ -solidifying Ti-44Al alloy was characterized by random orientations of the lamellae in colonies (Fig. 3a) [4]. Obviously, during cooling subsequent to solidification, the  $\beta$  phase transformed into the  $\alpha$  phase with appearance of different orientation variants of  $\alpha$  and, upon following cooling, the random oriented lamellar microstructure arose. However, the microstructure of the Ti-44Al alloy still consisted of coarse colonies elongated along the heat-flow direction that should be ascribed to the low nucleation and rapid growth rates of  $\alpha$  during the solid-state  $\beta \Rightarrow \alpha$  transformation. Fig. 2b shows quantitative concentration line profile obtained for the binary Ti-45Al alloy. As is seen, only moderate dendritic segregation was observed in the

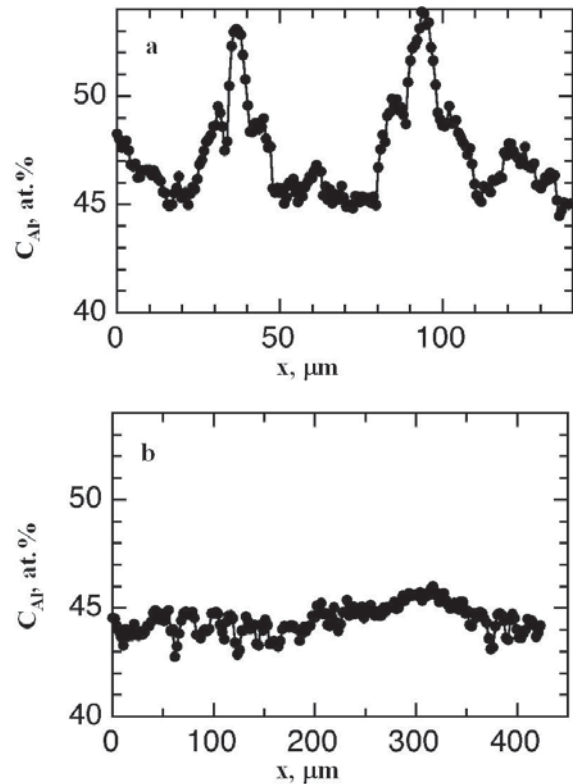
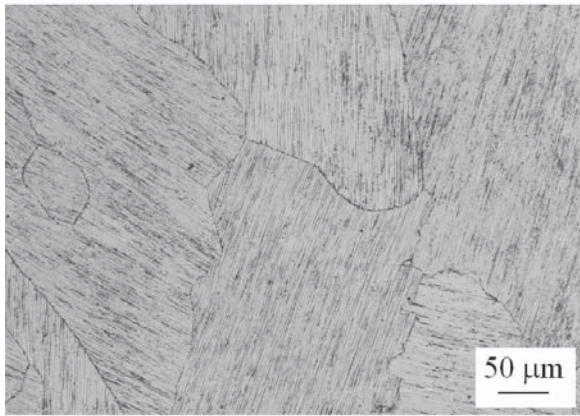


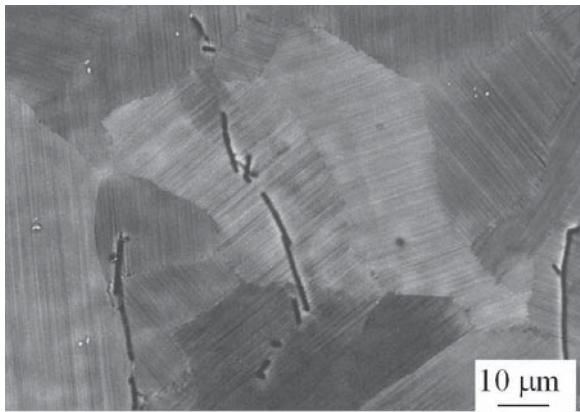
**Fig. 2.** Quantitative concentration line profiles as obtained by EDX analysis from the upper part of arc-melted buttons. (a) Ti-48Al, (b) Ti-45Al. The distribution of aluminum in the Ti-48Al alloy solidifying through peritectic reactions is much more inhomogeneous than that in the  $\beta$ -solidifying Ti-45Al alloy.

button of the alloy, that is,  $\beta$ -solidifying alloys are more preferable from the viewpoint of chemical homogeneity than alloys solidifying through the peritectic reactions.

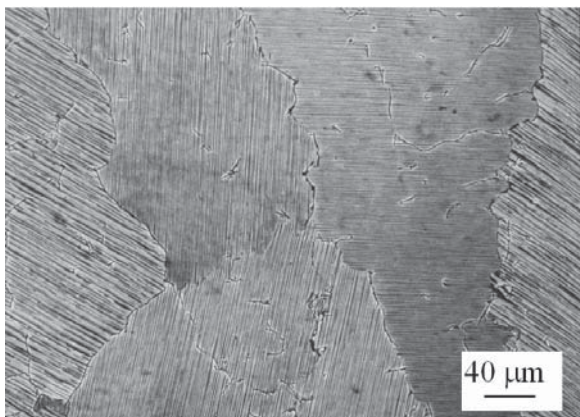
Thus,  $\beta$ -solidifying alloys are of great interest because they have a potential for producing sound castings with a chemically homogeneous microstructure free of sharp casting texture. Furthermore, it seems that the as-cast microstructure might be refined due to realization of many orientation variants of  $\alpha$  during the solid-state  $\beta \Rightarrow \alpha$  transformation. To this end, one should increase the nucleation rate of  $\alpha$  and decrease its growth rate. Besides, the refined microstructure is bound to be retained on passing through the single  $\alpha$  phase. Further, these problems are to be considered.



a)



b)



c)

**Fig. 3.** Microstructures of  $\beta$ -solidifying alloys. (a) Ti-44Al and (b, c) Ti-44Al-0.2B in (a, b) the as-cast condition, (c) after additional annealing at  $T=1450$  °C, followed by furnace cooling. The heat-flow direction is vertical. The lamellae are observed to have multiple orientations. (a) Optical microscopy, (b,c) scanning electron micrographs taken in the back-scattering electron mode.

### 3.2. Microstructural refinement of $\beta$ -solidifying $\gamma+\alpha_2$ alloys by boron additions

Boron additions are known to act as an effective grain-refining agent in  $\gamma+\alpha_2$  alloys [11-13]. When solidification occurs, borides (predominantly  $TiB_2$  [11,13]) arise that can both refine the ingot microstructure and restrict growth of a grains upon heating in the  $\alpha$  phase field, especially in case of hot worked material, in that borides are broken up [11,14,15]. DSC analysis of the boron doped Ti-44Al alloy showed that the solidification and solid-state transformation pathway was:  $L \Rightarrow \beta \Rightarrow \alpha + \beta \Rightarrow \alpha \Rightarrow \alpha + \gamma \Rightarrow \alpha_2 + \gamma$  (Table 1). Note that boron additions led to a slight increase in the eutectoid and  $\alpha$ -transus temperatures and to a slight decrease in the  $(\alpha+\beta)$ -transus temperature. In other words, the boron additions acted as a  $\beta$ -stabilizing element.

The boron additions gave rise to a significant refinement of initial as-cast microstructure as compared with the binary Ti-44Al alloy. Lamellar colonies had an elongated shape with a length of 50-60  $\mu m$  and a width of 20-30  $\mu m$  and consisted of the thin lamellae (Fig. 3b). Different lamellae orientations were observed in the microstructure. However, a set of these orientations was limited and many colonies had the same orientation. Such type of microstructure can be called 'parquet'. The lamellae orientation in each colony was predominantly perpendicular to the growth direction that indicates a preferable growth of  $\alpha$  grains along the  $c$  axis during the solid-state  $\beta \Rightarrow \alpha$  transformation. Thus, borides increased the rate of heterogeneous nucleation of  $\alpha$  during the  $\beta \Rightarrow \alpha$  transformation that promoted refinement of the microstructure. As a result, instead of a coarse columnar structure and sharp casting texture typical of cast  $\gamma+\alpha_2$  alloys [16], the 'parquet' microstructure with a relatively small colony size was obtained in the alloy (Fig. 3b). As one should expect, significant dendritic segregation, which is a feature of alloy castings solidifying through the peritectic reactions, was not observed in this alloy.

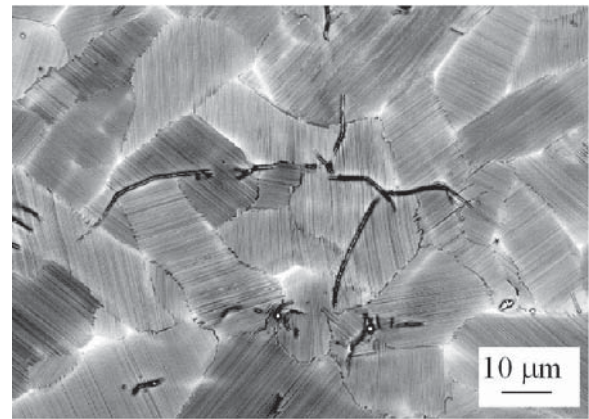
Furnace heating up to temperature as high as  $T=1450$  °C and annealing at this temperature during 5 min, followed by furnace cooling led to coarse colonies elongated along the heat-flow direction and to random lamellae orientations (Fig. 3c). Such heat treatment was carried out in order to imitate cooling conditions of a large-scale ingot. The coarsening of the ingot microstructure during the heat treatment can be connected with decreasing the nucleation rate of the  $\alpha$  phase and increasing its growth rate

during the  $\beta \Rightarrow \alpha$  transformation. Besides, coarsening of the ingot microstructure might occur on passing through the single  $\alpha$  phase field during cooling. A large number of boride ribbons in the colony interior suggest that they were not able to prevent from growing a grains during furnace cooling. Thus, a high growth rate of  $\alpha$  during the  $\beta \Rightarrow \alpha$  transformation and low stability of  $\alpha$  grains can hinder from producing a fine-grained microstructure in large-scale ingots of the Ti-44Al-0.2B alloy. Note that the grain-refining effect of boron additions is weaker in alloys solidifying through the peritectic reaction as compared to alloys solidifying through the  $\beta$  phase [11]. Probably, this is because of higher temperatures of the  $\alpha$  phase formation.

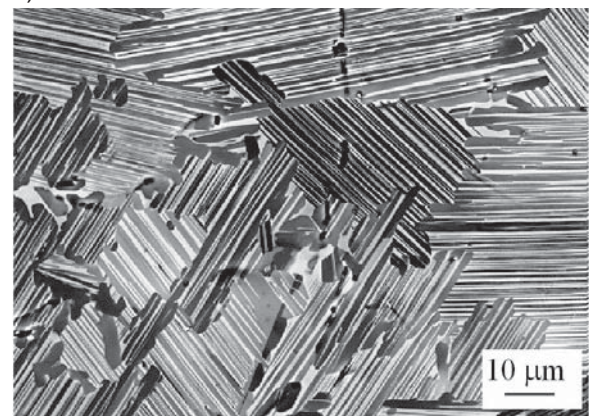
### 3.3. Microstructural refinement and stabilization of $\beta$ -solidifying $\gamma+\alpha_2$ alloys by doping of elements with a low diffusive mobility

In order to decrease the growth rate of the  $\alpha$  phase during the  $\beta \Rightarrow \alpha$  transformation and to increase the stability of  $\alpha$  grains, it is of interest to dope the elements with a low diffusive mobility. As has been shown recently, the most promising alloying element in this respect is niobium, which can be dissolved in both the  $\gamma$  and  $\alpha_2$  phases in amount of about 10 at.% [5, 17-19]. Niobium additions increase considerably the activation energy of diffusion in the  $\gamma$  and  $\alpha_2(\alpha)$  phases [18,19], that is, niobium additions may be used for decreasing the growth rate of  $\alpha$  during the  $\beta \Rightarrow \alpha$  transformation and increasing stability of  $\alpha$  grains on passing through the single  $\alpha$  phase field during cooling. It is also important that niobium additions lead to increasing corrosion resistance and high temperature strength of  $\gamma+\alpha_2$  alloys, facilitate deformation twinning because of decreasing the stacking fault energy in the  $\gamma$  phase that increases ductility of the alloys [17, 18]. Therefore, niobium additions appear to be valuable as for refinement and stabilization of the ingot microstructure as for improving high-temperature properties of boron doped  $\beta$ -solidifying  $\gamma+\alpha_2$  alloys.

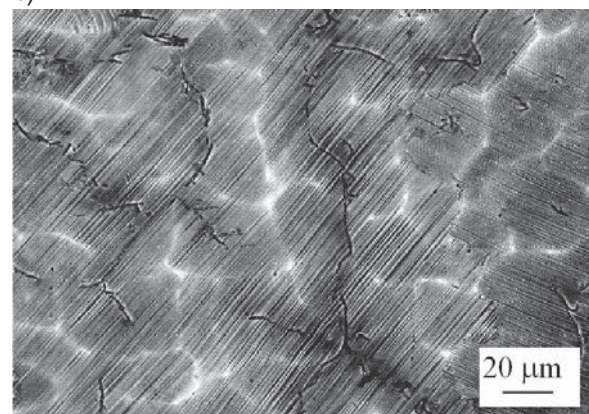
Doping of 5 at.% niobium led to a further increase in the eutectoid and a-transus temperatures and to a slight decrease in the  $(\alpha+\beta)$ -transus temperature as compared with those of the Ti-44Al-0.2B and Ti-44Al alloys (Table 1). As expected, the 'parquet' microstructure with a finer colony size than that in the case of the Ti-44Al-0.2B alloy was observed (Fig. 4a). A typical size of colonies in the Ti-44Al-5Nb-0.2B alloy amounted to 20-30 mm in length and 10-20 mm in width. BSE image of the microstructure



a)



b)



c)

**Fig. 4.** Microstructures of the (a, b) Ti-44Al-5Nb-0.2B and (c) Ti-46Al-5Nb-0.2B alloys in (a,c) as-cast conditions, (b) after additional annealing at  $T=1450$  °C, followed by furnace cooling. (a) The layers of the  $\beta$  phase located predominantly along colony boundaries are observed in the  $\beta$ -solidifying Ti-44Al-5Nb-0.2B alloy. (b) Dissolution of the  $\beta$  phase took place and some individual lamellae grew from one colony into the neighboring one. In the both alloys,  $\gamma$  grains arisen from  $\beta \Rightarrow \gamma$  transformation are seen along colony boundaries. (c) Dendrite microstructure is clearly distinguished in the microstructure of the Ti-46Al-5Nb-0.2B alloy solidifying through the peritectic  $L+\beta \Rightarrow \alpha$  reaction. Dendrite arms have a light contrast, interdendritic spacings have a dark contrast. The pictures were made by SEM in the back-scattering electron mode.

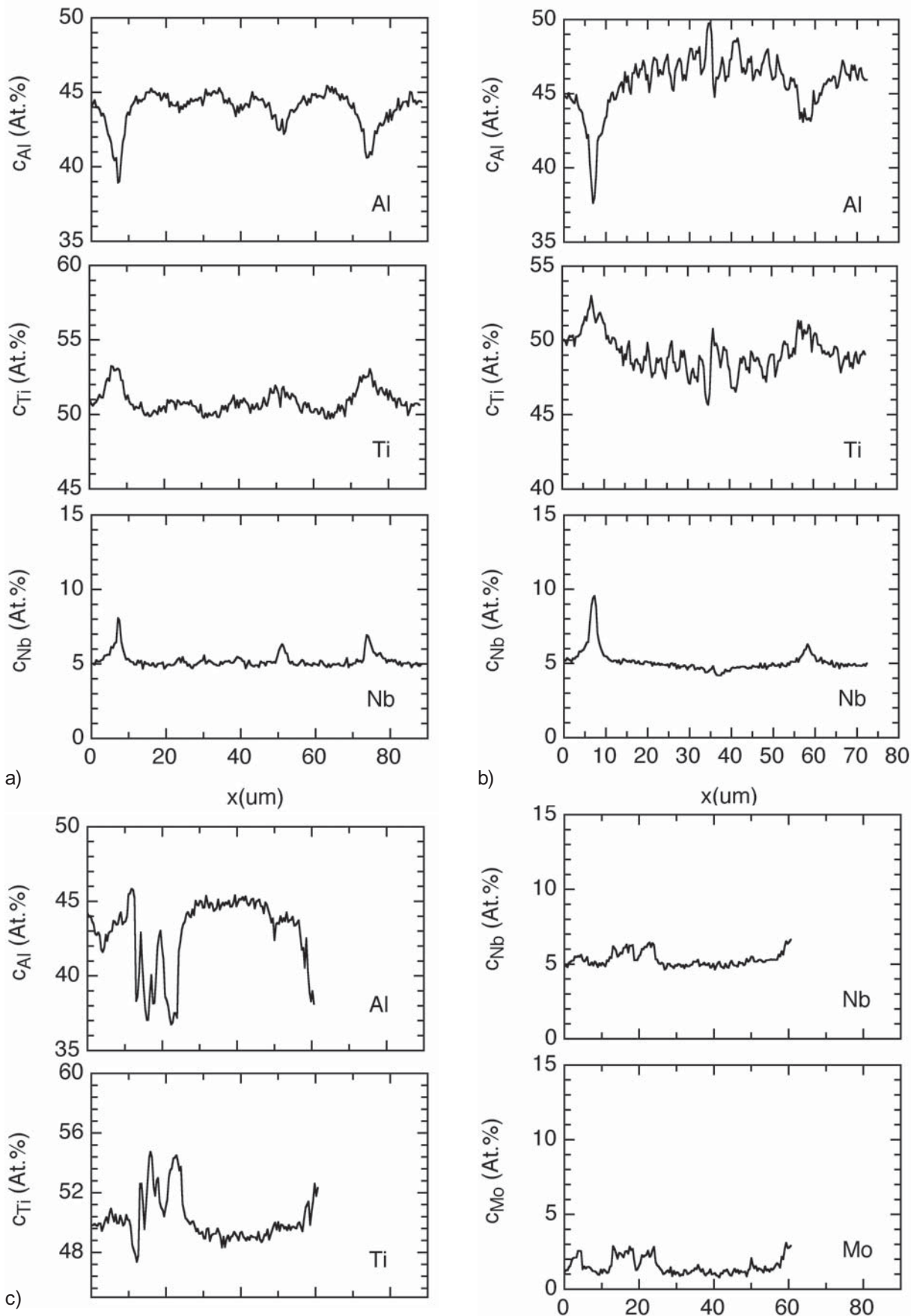


**Fig. 5.** Microstructure of the alloys (a) Ti-44Al-5Nb-0.2B, (b) Ti-46Al-5Nb-0.2B and (c) Ti-44Al-5Nb-1Mo-0.2B-0.3C and corresponding quantitative concentration line profiles obtained by EDX analysis. The concentrations profiles show the distribution of alloying elements along the lines marked on the microphotographs. Scanning electron micrographs taken in the back-scattering electron mode.

revealed light layers which formed a net (Fig. 4a). The layers had a thick of about 2 mm and were predominantly observed along colony boundaries. Quantitative EDX analysis showed that the layers were rich in niobium and titanium and depleted in aluminum (Fig. 5a). The segregation formation was a result of the rejection of the  $\beta$  stabilizing elements into the  $\alpha/\beta$  interphase boundaries during the  $\beta \Rightarrow \alpha$  transformation. This was confirmed by predominant location of the net along colony boundaries. The same conclusion was made under investigation of the Ti-44Al-8Nb-1B, Ti-44Al-4Nb-4Zr-0.2Si-1B and Ti-44Al-4Nb-4Ta-0.2Si-1B alloys [20]. Since the  $\beta$  phase contains more niobium [21] and has comparatively open BCC structure in comparison with the  $\alpha$  phase, it should be expected that redistribution of elements in the  $\beta$  phase occurred faster than that in the  $\alpha$  phase. Thus, results of the EDX analysis indicated that the light layers were the  $\beta$  phase, which was retained upon cooling down to room temperature.

Furnace cooling after annealing at  $T=1450$  °C led to some coarsening of the microstructure as compared with the initial as-cast condition (Fig. 4b). The mean colony size increased to 70  $\mu\text{m}$ , the colonies became equiaxed and lamellar spacings increased. In contrast to the as-cast condition, in the heat-treated condition, the  $\beta$  phase was not retained upon cooling down to room temperature, that is, the  $\beta$  phase was metastable. Small  $\gamma$  grains were frequently observed along lamellar colonies suggesting that they were a result of the  $\beta \Rightarrow \gamma$  transformation during cooling [20-24]. It is also seen that some individual lamellae grew from one colony into the neighboring one. The mechanism of such growing was described in Ref. [24].

When comparing experimental results obtained for the Ti-44Al-0.2B and Ti-44Al-5Nb-0.2B alloys, one may conclude that the colony size in the as-cast conditions was mainly determined by stability of  $\alpha$  grains on passing through the single  $\alpha$  phase field. In fact, the colony size in the buttons of both the alloys did not significantly differ while the heat treatment resulted in a drastic difference in the colony size of the alloys. In all probability, the metastable  $\beta$  phase impeded the  $\alpha$  grain growth during furnace cooling that gave rise to much finer colony size in the Ti-44Al-5Nb-0.2B alloy as compared with that in the Ti-44Al-0.2B alloy. In addition, it seems that niobium additions decreased the growth rate of the  $\alpha$  phase during the  $\beta \Rightarrow \alpha$  transformation that also might contribute to the decrease in the  $\alpha$  grain size.

Thus, a significant microstructural refinement, which was observed upon cooling of the Ti-44Al-5Nb-

0.2B button, seems to be feasible for large-scale ingots. For that,  $\beta$ -solidifying alloys doped with boron and elements with a low diffusive mobility like niobium should be selected. Besides, the doped elements should be located predominantly in the  $\beta$  phase to provide both the formation of segregation of these elements along the  $\alpha/\beta$  interphase boundaries during the  $\beta \Rightarrow \alpha$  transformation and the increase in stability of the  $\beta$  phase along  $\alpha$  grains during subsequent cooling, that is, the doped elements should have a high partition coefficient  $k_{\beta/\alpha} = X_{\beta}/X_{\alpha}$ , where  $X_{\alpha}$  and  $X_{\beta}$  are equilibrium mole fractions of doped elements in the  $\alpha$  and  $\beta$  phases. Obviously, the higher amount of the metastable  $\beta$  phase the higher stability of  $\alpha$  grains. DSC analysis and microstructural investigation of the Ti-44Al-5Nb-0.2B alloy showed the following phase transformation sequence during cooling:  $L \Rightarrow L + \beta \Rightarrow \beta \Rightarrow \alpha + \beta \Rightarrow \alpha + \beta_m \Rightarrow \alpha + \gamma + \beta_m \Rightarrow \alpha_2 + \gamma + \beta_m$ , where  $\beta_m$  is the metastable  $\beta$  phase.

It is of interest to compare the ingot microstructures of a  $\beta$ -solidifying alloy and an alloy solidifying through the peritectic reaction. Fig. 4c represents the ingot microstructure of the Ti-46Al-5Nb-0.2B alloy. Lamellar colonies elongated along the heat-flow direction with a length of up to 1000 mm were observed. Dendritic structure was clearly distinguished. Dendrite arms had a light contrast whereas interdendritic spacings had a dark contrast. Note that the lamellae were oriented at angle of 0, 45 or 90° with respect to the primary dendrite arms. As is seen in Fig. 4c, only one or sometimes two orientations of 12 possible orientations of the  $\alpha$  phase were realized around each dendrite. The observed orientations of the lamellae with respect to the primary dendrite arms were detected earlier in the Ti-50Al-6Mo alloy [10]. Quantitative EDX analysis revealed that the dendrite arms were rich in niobium, titanium and depleted in aluminum whereas the interdendritic regions were rich in aluminum (Fig. 5b). It may be concluded, therefore, that the  $\beta$  phase was located in the dendritic arms. Because of the above microstructural features, the Ti-46Al-5Nb-0.2B alloy can be identified as an alloy solidifying through the  $L + \beta \Rightarrow \alpha$  peritectic reaction. The following sequence of phase transformations took place during its cooling:  $L \Rightarrow L + \beta_c \Rightarrow \alpha + \beta_c \Rightarrow \alpha + \gamma + \beta_c \Rightarrow \alpha_2 + \gamma + \beta_c$ , where  $\beta_c$  is the dendritic core of the  $\beta$  phase (Table 1) [25]. Thus, the ingot microstructure of such alloy contained significant chemical inhomogeneities caused by dendritic segregation and could not be refined using the  $\beta \Rightarrow \alpha$  transformation.

### 3.4. Additional microstructural refinement and stabilization of $\beta$ -solidifying $\gamma+\alpha_2$ alloys by doping of elements which provide a high partition coefficient between the $\beta$ and $\alpha$ phases and a decrease in the rate of diffusion in the $\alpha$ phase

For further decreasing the  $\alpha$  grain size, either additional increasing niobium content (for instance, as high as 8-10%) in the base-line composition Ti-44Al-5Nb-0.2B or doping of such elements as molybdenum and tungsten can be used. An additional increase in niobium content seems to be inexpedient because molybdenum and tungsten, according to literature data, have much higher partition coefficient  $k_{\beta/\alpha}$  than that of niobium [22] and, therefore, these elements can be doped in a small amount to provide higher stability of the metastable  $\beta$  phase and a smaller  $\alpha$  grain size. Just as niobium, these doping elements increase the activation energy of diffusion in both the  $\gamma$  and  $\alpha_2$ (a) phases [7,13] and high temperature strength and creep resistance. Moreover, in contrast to niobium, these doping elements increase the fraction of the  $\gamma$  phase in  $\gamma+\alpha_2$  alloys [22] that is important from the viewpoint of ductility at room temperature since the  $\gamma$  phase is more ductile than the  $\alpha_2$  phase [4]. In the present paper, an effect of molybdenum on stability of the  $\beta$  phase and the  $\alpha$  grain size will be considered (an effect of tungsten is similar).

In order to decrease the growth rate of  $\alpha$  grains on passing through the single  $\alpha$  phase field, doping of carbon seems to be also useful. According to Ref. [26], carbon segregates on the  $\alpha$  grain boundaries and decreases the rate of diffusion in the  $\alpha$  phase. It should be also noted that due to formation of carbides,  $\gamma+\alpha_2$  alloys exhibited enhanced high-temperature capability at intended service temperatures ( $T=600-800$  °C) in comparison with alloys being free of carbon [17,18].

The composition of the Ti-44Al-5Nb-1Mo-0.2B-0.3C alloy was selected reasoning from the two conditions. First, the composition ensured  $\beta$  solidification. Here we account for the fact that such strong  $\beta$  and  $\alpha$  stabilizing elements as molybdenum and carbon, respectively, displaced the binary diagram boundaries in the opposite directions. Second, the composition provided the presence of the single  $\alpha$  phase field indicating that the above mentioned phase transformation sequence was:  $L \Rightarrow L+\beta \Rightarrow \beta \Rightarrow \alpha+\beta \Rightarrow \alpha+\beta_m \Rightarrow \alpha+\gamma+\beta_m \Rightarrow \alpha_2+\gamma+\beta_m$  (Table 1).

The ingot microstructure of the Ti-44Al-5Nb-1Mo-0.2B-0.3C alloy was also of 'parquet' type with a

typical length and width of 30-35 and 20-25  $\mu\text{m}$  respectively (Fig. 6a). Additions of molybdenum resulted in thickening of the  $\beta$  layers, which amounted to 4-5  $\mu\text{m}$ . Quantitative EDX analysis revealed that molybdenum had a more strong tendency to form segregations in the layers in comparison with niobium (Fig. 5c), that is, actually, molybdenum was characterized by a higher partition coefficient  $k_{\beta/\alpha}$  than that of niobium. The net of the  $\beta$  phase located predominantly along the colony boundaries and only some  $\beta$  layers intersected the colonies (Fig. 6a). The latter might decorate the former interphase  $\alpha/\beta$  boundaries or represent the dendrite arms. In the interior of the  $\beta$  phase layers, the  $\gamma$  phase was observed.  $\gamma$  grains were either alternated with  $\beta$  grains or precipitated in the form of the needle-shaped lamellae. According to Ref. [24], the mixture of  $\beta$  and  $\gamma$  grains might be resulted from the cellular reaction  $\beta \Rightarrow \beta+\gamma$ , whereas the needle-shaped  $\gamma$ -lamellae might arise due to the solid-state  $\beta \Rightarrow \gamma$  transformation.

Furnace cooling after annealing at  $T=1450$  °C led to the formation of the fine-grained 'parquet' microstructure with the mean colony size of 30  $\mu\text{m}$  (Fig. 6b). The  $\beta$  phase dissolved partially turning into the  $\gamma$  phase, therefore, both the mixture of  $\beta$  and  $\gamma$  grains and individual  $\gamma$  grains were observed along the colony boundaries. As seen from Fig. 6c, some individual lamellae grew from one colony into the neighboring one but this effect was pronounced to a lesser extent than that in the Ti-44Al-5Nb-0.2B alloy. A smaller colony size in the Ti-44Al-5Nb-1Mo-0.2B-0.3C alloy in comparison with that in the Ti-44Al-5Nb-0.2B alloy can be ascribed to influence of molybdenum and carbon. The former favored decreasing the growth rate of  $\alpha$  grains during the  $\beta \Rightarrow \alpha$  transformation that was obviously caused by decreasing the rate of diffusion. Having a higher partition coefficient  $k_{\beta/\alpha}$  than niobium, molybdenum stabilized a higher amount of the  $\beta$  phase along  $\beta$  grain boundaries decelerating its dissolution and, hence, hindering from growing  $\alpha$  grains on passing through the single  $\alpha$  phase field. The additions of carbon seemed to impede the growth of  $\alpha$  grains as well because they might both segregate on the  $\alpha$  grain boundaries and decrease the rate of diffusion in the  $\alpha$  phase [26].

An approach demonstrated for the Ti-44Al, Ti-44Al-0.2B, Ti-44Al-5Nb-0.2B and Ti-44Al-5Nb-1Mo-0.2B-0.3C alloys was used for the development of a new class of  $\beta$ -solidifying  $\gamma+\alpha_2$  alloys (not presented here) which had chemically homogeneous fine-grained microstructure in as-cast condition and contained the metastable  $\beta$  phase. Since the  $\beta$  phase



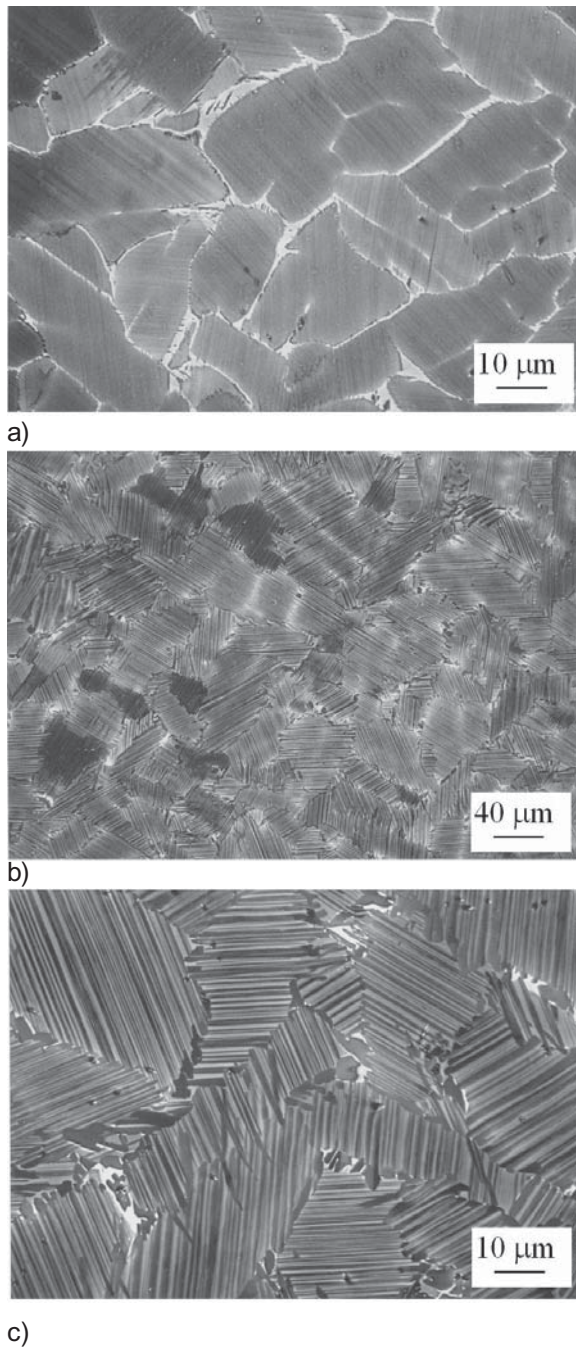


**Fig. 6.** Microstructures of the alloy Ti-44Al-5Nb-1Mo-0.2B-0.3C alloy in (a) the as-cast condition, (b, c) after an additional annealing at  $T=1450\text{ }^{\circ}\text{C}$ , followed by furnace cooling. (a) Layers of the  $\beta$  phase are located along colony boundaries and sometimes in the colony interior. (b) Furnace cooling led to the formation of a quite homogeneous and fine-grained microstructure with a mean colony size of about 30  $\mu\text{m}$ . (c) The growth of some individual lamellae from one colony into the neighboring one is pronounced to a lesser extent than in the Ti-44Al-5Nb-0.2B alloy. Scanning electron micrographs taken in the back-scattering electron mode.

is significantly softer than the  $\gamma$  and  $\alpha_2$  phases, these alloys demonstrated high workability. Mechanical behavior and microstructural evolution on hot working of these alloys will be considered in coming future. A valuable feature of new alloys is the fact that after hot working the  $\beta$  phase can be easily dissolved during final heat treatment to provide in this way desirable mechanical properties from the viewpoint of subsequent high-temperature service.

#### 4. CONCLUSIONS

A novel alloy designing concept addressed on the production of sound  $\gamma$ -TiAl+ $\alpha_2$ -Ti<sub>3</sub>Al alloy castings with a chemically homogeneous fine-grained microstructure has been proposed. The concept is based on efficient alloying which provides: i) solidification through the  $\beta$  phase to initiate different orientation variants of the  $\alpha$  phase; ii) an increase in the rate of heterogeneous nucleation of the  $\alpha$  phase during the  $\beta \Rightarrow \alpha$  phase transformation owing to the boron additions and a decrease in its growth rate due to the niobium and molybdenum additions having a low diffusive mobility; iii) an increase in stability of  $\alpha$  grains on passing through the single  $\alpha$  phase field during cooling owing to the niobium, molybdenum, boron and carbon additions. The additions of niobium and especially molybdenum stabilized the  $\beta$  phase along  $\alpha$  grains and prevented from their growing on passing through the single  $\alpha$  phase field during cooling. The boron additions led to formation of borides which might anchor the  $\alpha$  grain boundaries. The additions of carbon seemed to impede the growth of  $\alpha$  grains as well because they might both segregate on the  $\alpha$  grain boundaries and decrease the rate of diffusion in the  $\alpha$  phase. The obtained results offer the challenge in the development of new  $\gamma+\alpha_2$  alloys with improved workability and a good high temperature capability.

#### REFERENCES

- [1] P.L. Martin, D.A. Hardwick, D.R. Clemens, W.A. Konkel and M.A. Stucke, In: *Structural Intermetallics*, ed. by M.V. Nathal *et al.* (The Minerals, Metals & Mater. Soc. 1997) p.387.
- [2] S.L. Semiatin, J.C. Chesnutt, C. Austin and V. Seetharaman, In: *Structural Intermetallics*, ed. by M.V. Nathal *et al.* (The Minerals, Metals & Mater. Soc. 1997) p.263.
- [3] D.M. Dimiduk, P.L. Martin and Y-W. Kim // *Mater. Sci. Eng.* **A243** (1998) 66.
- [4] S. Naka, M. Thomas, C. Sanchez and T. Khan, In: *Structural Intermetallics*, ed. by M.V.

- Nathal *et al.* (The Minerals, Metals & Mater. Soc. 1997) p.313.
- [5] U. Brossman, M. Oehring and F. Appel, In: *Structural Intermetallics*, ed. by K.J. Hemker *et al.* (The Minerals, Metals & Mater. Soc. 2001) p.191.
- [6] K.B. Povarova, O.A. Bannyh, I.V. Burov *et al.* // *Metals* **3** (1998) 31, In Russian.
- [7] Y-W. Kim and D.M. Dimiduk, In: *Structural Intermetallics*, ed. by M.V. Nathal *et al.* (The Minerals, Metals & Mater. Soc. 1997) p.531.
- [8] R.M. Imayev, V.M. Imayev, M. Oehring and F. Appel // *Met. Trans.* **36A** (2005) 859.
- [9] C. McCullough, J.J. Valencia, C.G. Levi and R. Mehrabian // *Acta Met.* **37** (1989) 1321.
- [10] A.K. Singh, K. Muraleedharan and D. Banerjee // *Scr. Mater.* **48** (2003) 767.
- [11] Y-W. Kim and D.M. Dimiduk, In: *Structural Intermetallics*, ed. by K.J. Hemker *et al.* (The Minerals, Metals & Mater. Soc. 2001) p.625.
- [12] B.J. Inkson, C.B. Boothroyd and C.J. Humphreys // *Acta Mater.* **43** (1995) 1429.
- [13] M. De Graef, D.A. Hardwick and P.L. Martin, In: ed. by M.V. Nathal *et al.* (The Minerals, Metals & Mater. Soc. 1997) p.185.
- [14] V.M. Imayev, R.M. Imayev and A.V. Kuznetsov // *Scr. Mat.* **49** (2003) 1047.
- [15] A.V. Kuznetsov, V.M. Imayev and R.M. Imayev // *Metals* **6** (2002) 102, In Russian.
- [16] H. Mecking and Ch. Hartig, In: *Gamma Titanium Aluminides*, ed. by Y-W. Kim, R. Wagner and M. Yamaguchi, (The Minerals Metals and Mater. Soc. 1995) p.525.
- [17] F. Appel, M. Oehring and R. Wagner // *Intermetallics* **8** (2000) 1283.
- [18] F. Appel, M. Oehring, J.D.H. Paul and U. Lorenz, In: *Structural Intermetallics*, ed. by K.J. Hemker *et al.* (The Minerals, Metals & Mater. Soc. 2001) p.63.
- [19] Chr. Herzig, T. Przeorski, M. Friesel, F. Hisker and S. Divinski // *Intermetallics* **9** (2001) 461.
- [20] T.T. Cheng, In: *Gamma Titanium Aluminides*, ed. by Y-W. Kim, D.M. Dimiduk and M.H. Loretto (The Minerals, Metals and Mater. Soc. 1999) p.389.
- [21] G.L. Chen, W.J. Zhang, Z.C. Liu and S.J. Li, In: *Gamma Titanium Aluminides*, ed. by Y-W. Kim, D.M. Dimiduk and M.H. Loretto (The Minerals, Metals and Mater. Soc. 1999) p.371.
- [22] R. Kainuma, Y. Fujita, H. Mitsui, I. Ohnuma and K. Ishida // *Intermetallics* **8** (2000) 855.
- [23] T.T. Cheng and M.H. Loretto, In: *Structural Intermetallics*, ed. by M.V. Nathal *et al.* (The Minerals, Metals & Mater. Soc. 1997) p.253.
- [24] Z. Zhang, K.J. Leonard, D.M. Dimiduk and V.K. Vasudevan, In: *Structural Intermetallics*, ed. by K.J. Hemker *et al.* (The Minerals, Metals & Mater. Soc. 2001), CD edition.
- [25] M. Krishnan, B. Natarajan, V.K. Vasudevan and D.M. Dimiduk, In: ed. by M.V. Nathal *et al.* (The Minerals, Metals & Mater. Soc. 1997) p.235.
- [26] H.S. Park, S.W. Nam, N.J. Kim and S.K. Hwang // *Scr. Mater.* **41** (1999) 1197.